INORGANIC CHEMISTRY
FRONTIERS

RESEARCH ARTICLE

View Article Online
View Journal

Cite this: DOI: 10.1039/c9qi01509d

Hydrogen peroxide disproportionation with manganese macrocyclic complexes of cyclen and pyclen†

David M. Freire, [a] Debora Beeri, [a] Kristof Pota, [a] Hannah M. Johnston,[a] Philip Palacios,[b] Brad S. Pierce, [c] Benjamin D. Sherman [a] and Kayla N. Green *[a]

Received 21st November 2019,
Accepted 21st February 2020

DOI: 10.1039/c9qi01509d

rsc.li/frontiers-inorganic

The catalase family of enzymes, which include a variety with a binuclear manganese active site, mitigate the risk from reactive oxygen species by facilitating the disproportionation of hydrogen peroxide into molecular oxygen and water. In this work, hydrogen peroxide disproportionation using complexes formed between manganese and cyclen or pyclen were investigated due to the spectroscopic similarities with the native MnCAT enzyme. Potentiometric titrations were used to construct speciation diagrams that identify the manganese complex compositions at different pH values. Each complex behaves as a functional mimic of catalase enzymes. UV-visible spectroscopic investigations of the H_2O_2 decomposition reaction yielded information about the structure of the initial catalyst and intermediates that include monomeric and dimeric species. The results indicate that rigidity imparted by the pyridine ring of pyclen is a key factor in increased TON and TOF values measured compared to cyclen.

Introduction

Oxidative stress results from an imbalance between reactive oxygen species (ROS) and the availability/activity of antioxidants.[1] Hydrogen peroxide and the hydroxyl radical ($OH^{\bullet}$), formed after the one electron reduction of the former, are examples of ROS involved in Fenton or Haber–Weiss type reactions that occur between redox active transition metal ions and molecular oxygen. The high chemical reactivity of ROS and wide availability of the chemical precursors in biology make these species a threat to multiple types of tissues and cells and thereby contribute to the development of neurodegenerative, pulmonary, and cardiovascular diseases as well as promote a number of inflammation pathways.[1–10] The catalase family of enzymes mitigate the risk from ROS by facilitating the disproportionation of H_2O_2 into molecular oxygen and water. While most catalase enzymes contain an iron-protoporphyrin IX prosthetic group, some bacteria accomplish H_2O_2 decomposition *via* a catalase (MnCAT) with an active site that consists of a dinuclear manganese core bridged by carboxylate and single-atom ligands, likely water or hydroxide.[11–14]

Both structural and functional models of MnCAT have been produced as a result of the importance of this enzyme activity and interesting active site.[15] Many of these biomimetic complexes are dimeric in nature. Examples of binuclear manganese-oxo (Mn_2O_2) bridged species with a range of manganese oxidation states are also abundant and provide a rich history as models for the oxygen-evolving complex (OEC) in photosystem II.[16,17] However, only a small subset of monomeric manganese complexes have been isolated and reported to catalyze H_2O_2 disproportion; of these, few can function in aqueous solution or maintain activity across a range of pH values.[15,18]

The di-μ-oxo bridged manganese dimer of cyclen was first reported in 1988 by Brewer and co-workers and shown to provide water oxidation reactivity in acetonitrile.[19] In 2005, a modified synthesis and detailed characterization of $[Mn_2(cyclen)_2(\mu\text{-}O)_2][ClO_4]_3{\cdot}4H_2O$ was reported.[20] The authors noted the resemblance of the IR and electronic spectra with those reported for MnCAT but no reactivity toward H_2O_2 decomposition has been reported to date. Likewise and described herein, our exploration of the coordination chemistry of pyridinophane molecules like pyclen revealed that the EPR spectrum of $[Mn_2(pyclen)_2(\mu\text{-}O)_2][ClO_4]_3$ resembles that of MnCAT. The similarities in electronic structure with the native

[a]Department of Chemistry and Biochemistry, Texas Christian University, 2950 W. Bowie, Fort Worth, TX 76129, USA. E-mail: kayla.green@tcu.edu
[b]Department of Chemistry and Biochemistry, The University of Texas at Arlington, 700 Planetarium Place, Arlington, TX 76019, USA
[c]Department of Chemistry and Biochemistry, University of Alabama, 250 Hackberry Lane, Box 870336 Tuscaloosa, AL 35487, USA

†Electronic supplementary information (ESI) available: Spectroscopy and details of methods. CCDC 1963104 and 1963105. For ESI and crystallographic data in CIF or other electronic format see DOI: 10.1039/c9qi01509d

enzyme motivated the investigation of these complexes as H_2O_2 disproportionation catalysts presented here. Comparison of the reactivity with other macrocyclic forerunners illustrates the relationship between activity and the rigidity of the tetraazamacrocyclic core and helps to explain why nature utilizes a rigid polypyrrole macrocyclic core in MnCAT to achieve high catalytic activity.

Results and discussion

Recent reports of mononuclear 12-membered Mn(II)Py_2N_2 complexes that were functional mimics of MnCAT for the decomposition of H_2O_2 motivated the synthesis and study of pyclen derivatives herein.[18,21,22] While pyclen binds to a range of metal ions, complexes of pyclen with manganese have not been reported to date.[23–26] To assess Mn(II) complexation to pyclen and cyclen in a mononuclear form, potentiometric titrations were carried out in aqueous conditions at 25 °C with I = 0.15 M NaCl to emulate biological conditions. The log β and species distribution for Mn(II) with cyclen and pyclen were evaluated and results shown in Table 1 and Fig. 1, respectively. The formation of Mn(III)$(OH)_3$(s) and Mn_2O_3(s) precludes potentiometric titrations of the macrocyclic ligands in the presence of manganese(III) species. Therefore, the corresponding stability of Mn(III)pyclen were calculated using eqn (1) and cyclic voltammetry (CV) data.[27–29] No CV response was observed for the cyclen complex, which prohibited consideration of Mn(III)cyclen.

$$\Delta E_{1/2} = E_{1/2,\,\mathrm{complex}} - E_{1/2,\,\mathrm{Mn_{aq}}} = 0.59 \log \frac{\beta_{\mathrm{ox}}}{\beta_{\mathrm{red}}} \quad (1)$$

Overall, the manganese complex with pyclen is thermodynamically more favorable than that with cyclen. Based on the speciation diagrams (Fig. 1), 99% of the Mn(II) ions are complexed by pyclen at pH 8.1, while the cyclen congener reaches a maximum of 91% at pH 8.8. However, the Mn(II) L(OH) species (Table S2†) is modeled to be the predominate species at slightly more basic conditions (pH > 8.5) and prevents complete complexation of Mn(II) by cyclen in the bis-aquo form. This observation is consistent with that of other dinuclear μ-oxo complexes formed under basic conditions.[30]

The potentiometric titrations prompted isolation of *bona fide* manganese complexes of pyclen and cyclen. [Mn(pyclen)Cl_2][ClO_4] was produced by adding $Mn(ClO_4)_2$ to an aqueous solution of pyclen pre-adjusted to pH ~8 and stirred overnight under aerobic conditions (Fig. 2). A mononuclear cyclen complex was not isolable but is probable based on potentiometric data. The dinuclear [Mn_2(pyclen)$_2$(μ-O)$_2$][ClO_4]$_3$ was produced by co-dissolving pyclen with $Mn(ClO_4)_2$ in water and adjusting the pH of the mixture to ~8.[31] The [Mn_2(cyclen)$_2$

Table 1 Formation constants (log β_{pqr}) for compositions of [ML]/[M][L] for cyclen and pyclen with manganese ions

	$E^{o\prime}Mn^{III}/Mn^{II}$ *vs.* Fc^+/Fc(v)	$\Delta E^{o\prime}$	log β_{red} Mn(II)[b]	log β_{ox} Mn(III)[c]
[Mn(cyclen)]$^{2+}$	[a]	[a]	8.34(2)	[a]
[Mn(pyclen)]$^{2+}$	0.062	−0.114	10.11(4)	12.04

[a] Not measurable. [b] I = 0.15 M NaCl and T = 25.0 °C. [c] Derived from eqn (1) and $(Mn^{2+})_{aq}$, $E^{o\prime}Mn^{III}/Mn^{II}$ = 0.176 *vs.* $[Fe(CN)_6]^{3-}/[Fe(CN)_6]^{4-}$.

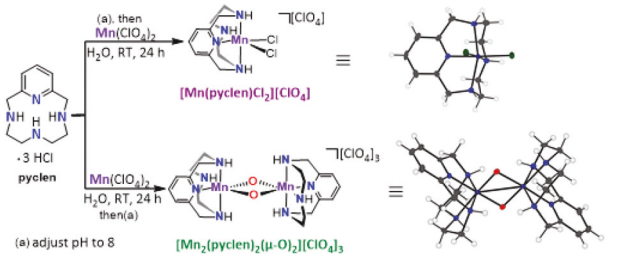

Fig. 2 Reaction conditions for the synthesis of monomeric [Mn(pyclen)Cl_2][ClO_4] and dimeric [Mn_2(pyclen)$_2$(μ-O)$_2$][ClO_4]$_3$ and the corresponding solid state structures determined by XRD analysis. Counter ions have been removed for clarity.

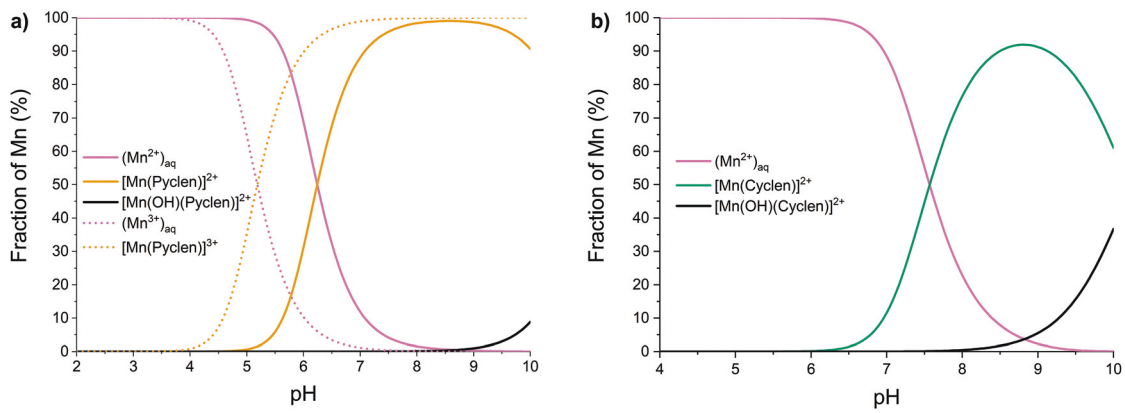

Fig. 1 Speciation diagram of (a) pyclen (10.00 mM) and (b) cyclen (10.00 mM) in the presence of 10 mM $MnCl_2{\cdot}4H_2O$ at I = 0.15 M NaCl and 25.0 °C.

$(\mu\text{-O})_2][ClO_4]_3\cdot 4H_2O$ complex was isolated using a previously published procedure.[19,20] In each case, the color of the solution developed into a deep green color after stirring overnight, open to air. The use of perchlorate salts facilitated the formation of crystalline materials, which were obtained by slow evaporation. The solid state structure of $[Mn_2(cyclen)_2(\mu\text{-O})_2][ClO_4]_3\cdot 4H_2O$ was reported previously and spectroscopic analysis agreed with the previous reports.[19,20] Therefore, only $[Mn(pyclen)Cl_2][ClO_4]$ and $[Mn_2(pyclen)_2(\mu\text{-O})_2][ClO_4]_3$ were evaluated by full spectroscopic and X-ray diffraction analysis. Bond lengths and angles for $[Mn(pyclen)Cl_2][ClO_4]$ and $[Mn_2(pyclen)_2(\mu\text{-O})_2][ClO_4]_3$ are available in Tables S4–S7.†

Spectroscopic analysis of $[Mn_2(pyclen)_2(\mu\text{-O})_2][ClO_4]_3$ in water showed a broad absorbance at 665 nm, a hallmark of a di-μ-oxo bridged dimer (Fig. S1†).[32,33] The absorbance bands at 555 and ~800 nm in aqueous solution correspond to the spin allowed $^5E_g \rightarrow {}^5T_{2g}$ transition of the Mn(III) ion and an intervalence transfer between the two manganese metal ions, respectively, based on literature precedent.[19,33–46] In addition, the Mn_2O_2 stretch for $[Mn_2(pyclen)_2(\mu\text{-O})_2][ClO_4]_3$ (683 cm^{-1}) is consistent with previous reports of similar complexes, including that of $[Mn_2(cyclen)_2(\mu\text{-O})_2][ClO_4]_3\cdot 4H_2O$ (689 cm^{-1}).[19]

Finally, the EPR spectra obtained for $[Mn_2(pyclen)_2(\mu\text{-O})_2][ClO_4]_3$ (Fig. 3 and Table S8†) exhibit a complex multiline hyperfine splitting pattern centered near g ~2.0 indicative of a ground $S = 1/2$ doublet. The observed 16-line hyperfine pattern and spin-state of these complexes closely match what has been reported for synthetic μ-oxo bridged $Mn^{III}Mn^{IV}$ clusters[47–50] as well as the $Mn^{III}Mn^{IV}$ state of Mn-catalase isolated from *Thermus thermophilus* (MnCAT).[11,48] In these systems, adjacent Mn^{III} ($S_1 = 2$) and Mn^{IV} ($S_2 = 3/2$) sites are strongly coupled antiferromagnetically resulting in a ground $S = 1/2$ spin-manifold. The bis-μ-oxo ligands bridging the $[Mn_2(pyclen)_2(\mu\text{-O})_2][ClO_4]_3$ cluster are expected to result in strong antiferromagnetic exchange coupling between manganese ions. Indeed, the temperature-normalized signal area follows Curie law behavior up to 100 K indicating that the energy gap separating the ground $S = 1/2$ doublet from the first excited $S = 3/2$ spin-manifold ($3J/2$) is beyond what can be depopulated thermally. This places a lower limit on the $Mn^{III}Mn^{IV}$ exchange coupling ($H = JS_1\cdot S_2$) of ~200 cm^{-1}.[51] It is therefore safe to treat the observed $Mn^{III}Mn^{IV}$ EPR spectra as originating from within an isolated $S = 1/2$ spin-manifold as described in eqn (2):

$$H_s = J(S_1 \cdot S_2) + \sum_{i=1,2} S_i \cdot D \cdot S_i + \beta(S_i \cdot g_i \cdot B) + S_i A_i I_i \quad (2)$$

where D and E are the axial and rhombic zero-field splitting parameters, g is the g-tensor, and J is the isotropic spin-exchange constant between two spin states. Analytical simulations of $[Mn_2(pyclen)_2(\mu\text{-O})_2][ClO_4]_3$ (Fig. 3, blue lines) were calculated from eqn (3) which faithfully reproduce multiline splitting, linewidth, and g- and A-values:

$$H_s = \beta(S_c \cdot g_i \cdot B) + S_c \cdot A \cdot I \quad (3)$$

where S_c represents the coupled spin state of the isolated manifold. A detailed analysis and summary of Mn^{III} and Mn^{IV} intrinsic g- and A-values for selected synthetic and enzymatic $Mn^{III}Mn^{IV}$-clusters is provided in ESI (Table S8†).

A one-pot approach for generating the Mn complex *in situ* was developed by taking advantage of the potentiometric titration data discussed above. As shown in Fig. 1, the pH ranges were determined where the majority of Mn^{2+} would be in the complexed form when in the presence of the given ligand (pH > 7.5 for cyclen; pH > 6.5 for pyclen with Mn^{2+}(aq.)). Fresh solutions were prepared from aqueous stock solutions containing $MnCl_2$ and cyclen or pyclen. For a given preparation, the reagent solutions were added to a starting volume of ultrapure water in the order of ligand, buffer, followed by Mn salt. Buffered solutions at pH 8.0 (Tris), 7.0 (HEPES), and 6.0 (citrate) were used. This one-pot approach avoided complications related with (1) the rapid formation of inactive Mn oxide/hydroxide species from the pre-synthesized and isolated samples upon re-dissolution and (2) the need to adjust the pH after adding the Mn(II) salt that would affect the relative concentration of the metal complex in solution.

Oxygen evolution measurements from the decomposition of H_2O_2 were carried out using 1.5 mM of $[Mn_2L_2(O)_2]^{3+}$ or $[MnLCl_2]^+$ and an O_2 microsensor probe (Unisense, Denmark) inserted into a hermetically sealed 15 mL reactor after flushing with nitrogen. Fig. S2† shows the setup used, which includes a snorkel to maintain 1 atm pressure within the cell. Addition of H_2O_2 (150 mM) resulted in obvious oxygen evolution based on the formation of bubbles in solution. For both manganese complexes of cyclen and pyclen, the introduction of H_2O_2 led to an immediate change in solution color (clear or light yellow to green) concomitant with the observation of gas evolution from solution. The microsensor used measures the partial pressure (concentration) of O_2 in contact with the probe and showed an increase in $[O_2]$ synchronized with the visual evolution of gas. Oxygen evolution plateaued after roughly 10–15 minutes for a given catalyst, and pH dependent calculated turnover numbers (TON) of 2.1 to 9.5 for the cyclen and

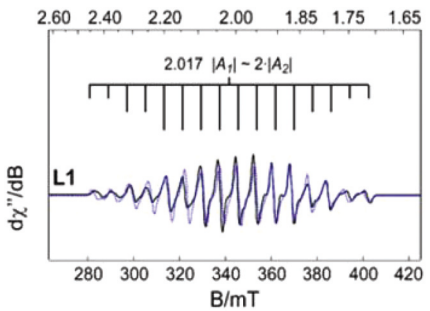

Fig. 3 X-band EPR spectra of $[Mn_2(pyclen)_2(\mu\text{-O})_2]^{3+}$ in water with 20% (v/v) glycerol. An analytical simulation (blue trace) for observed EPR data (black) for comparison. Instrumental parameters: microwave frequency 9.643 GHz; microwave power, 6 μW, modulation frequency 0.5 mT; modulation amplitude, 0.5 mT; temperature, 10 K. For clarity, simulation parameters utilized for each Mn_2(III,IV) cluster are summarized in Table S8.†

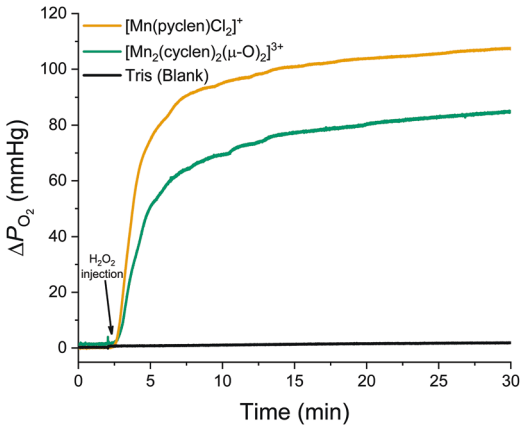

Fig. 4 Dioxygen formation from H_2O_2 disproportionation catalyzed by manganese complexes of cyclen (green) and pyclen (orange) at pH 8. The background generation of O_2 from H_2O_2 in the absence of complex, metal, or ligand is shown for reference (black). In each experiment, a concentrated sample of H_2O_2 was injected at t = 2.0 min to give $[H_2O_2]$ = 150 mM in the reactor. Initial conditions for generation of the given complex: $[Mn^{2+}]$ = 1.5 mM, [ligand] = 1.54 mM, [buffer] = 50 mM.

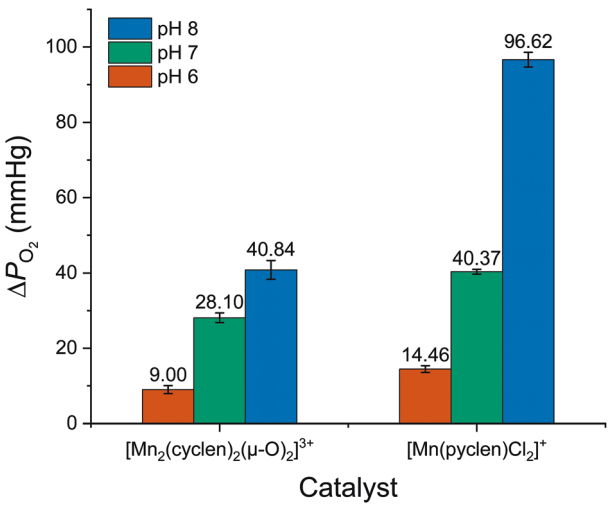

Fig. 5 ΔP_{O_2} from hydrogen peroxide disproportionation catalyzed by manganese complexes of cyclen and pyclen measured under different pH conditions. Initial conditions: $[Mn^{2+}]$ = 1.5 mM, [ligand] = 1.54 mM, $[H_2O_2]$ = 150 mM, [buffer] = 50 mM.

3.4 to 22.5 for the pyclen analog showed non-stoichiometric reactivity for H_2O_2 disproportionation (Fig. 5). Control reactions with ligand or metal alone showed a small increase in O_2 relative to that observed with the complexes and is attributed to the auto-disproportionation of H_2O_2 (Fig. S3†). Negligible H_2O_2 disproportionation in buffer alone is represented by the black trace in Fig. 4. These controls validate that the complex must be present for catalysis to occur.

For both $[Mn_2(cyclen)_2(\mu\text{-}O)_2]^{3+}$ and $[Mn(pyclen)Cl_2]^+$ the highest turnover number (TON) and turnover frequency (TOF) (Table 2) was observed at pH 8.0. Both the TON and TOF decreased gradually as the pH of the solution decreased. This is consistent with a decrease in the speciation of each complex with increasing acidity. While at pH 8, 76% and 98% of dissolved Mn^{2+} is in the form of $[MnLCl_2]^{2+}$, the proportion of complex decreases to 12% and 88% at pH 7 and 0% and 31% at pH 6 (for Mn(cyclen) and Mn(pyclen) complexes, respectively). Smith and co-workers have reported the Py_2N_2 pyridinophane congener of $[Mn(pyclen)Cl_2]$, which demonstrated a TON at pH 4 an order of magnitude greater than observed here. This suggests that structural differences are key to the relative activity of the Mn complex. Xu *et al.* also demonstrated that the addition of $-CH_3$ moieties to the non-aromatic N-atoms enhanced reactivity, while more bulky substituents (*t*-butyl, cyclohexyl) abolish any H_2O_2 disproportionation.[52] Taken in concert with the work here, activity increases with the number of pyridine (Py) moieties ($N_4 \rightarrow PyN_3 \rightarrow Py_2N_2$) in the macrocyclic ligand. Inclusion of pyridine moieties is known to enhance open-chain and macrocycle ligand rigidity and basicity, which has not been a consideration to date for catalytic reactions of this type.[53–55] Although the activities of the cyclen and pyclen complexes are lower in comparison to Py_2N_2 pyridinophanes, it is important to note that cyclen, a water oxidation catalyst,[19] is still active for H_2O_2 decomposition. Interestingly, $[Mn_2(pyclen)_2(\mu\text{-}O)_2][ClO_4]_3$ and $[Mn(pyclen)Cl_2][ClO_4]$ showed no water oxidation activity when we evaluated them under the same conditions. Moreover, cyclen–Mn readily forms μ-oxo dimers based on color changes observed in solution (the dimer has a characteristic green color). Conversion of the $[Mn(pyclen)Cl_2][ClO_4]$ to $[Mn_2(pyclen)_2(\mu\text{-}O)_2][ClO_4]_3$ proceeds similarly under comparable conditions. To further explore this phenomenon and relate it to the catalytic results, UV-visible spectroscopy was used to observe the Mn species present during the time course of the catalytic reaction.

Table 2 TON and TOF based on oxygen measurements recorded after the addition of H_2O_2 (150 mM) to solutions of the indicated manganese macrocyclic complexes formed *in situ*

	pH 6		pH 7		pH 8	
Mn complex	TON	TOF	TON	TOF	TON	TOF
Cyclen	2.1(2)	0.0194(7)[a]	6.5(3)	0.121(8)[b]	9.5(6)	1.23(5)[c]
Pyclen	3.4(2)	0.085(5)[b]	9.4(1)	0.88(4)[c]	22.5(5)	2.69(8)[c]

[a] TOF calculated at 100 min. [b] TOF calculated at 50 min. [c] TOF calculated at 10 min.

Spectroscopic investigations of $[Mn_2(cyclen)_2(\mu\text{-}O)_2]^{3+}$ and $[Mn(pyclen)Cl_2]^{+}$ mimicked the conditions used for H_2O_2 disproportion catalysis described above, however, a starting concentration of 2.0 mM $MnCl_2$ was used to ensure a strong UV-visible signal. The one-pot synthetic method was used to generate the given Mn complex at the start of the UV-visible absorption studies. Spectra of the ligand in the absence of Mn(II) salt showed elevated absorbance across the visible range, attributed to scattering, compared to the baseline taken of neat buffered solution (Fig. S6†). Upon addition of Mn(II) to an air saturated solution containing the ligand and buffer, an initial return to baseline followed by a gradual increase in absorbance in the visible range occurred over ten minutes (Fig. S5 and S6†). In the case of cyclen, a shift and increase in strong absorbance for $\lambda < 375$ nm indicates coordination of Mn with corresponding appearance of the ligand-to-metal charge transfer band of the complex. Over the 30 min aging period (Fig. S5†), features appear at 403 (sh) and 710 nm (attributed to Mn^{III} d–d transitions) similar to that observed for $[Mn^{III}\text{–}(\mu\text{-}O)_2\text{–}Mn^{III}]^{2+}$ species.[44,46,56] At longer aging times (~30 min), subtle growth in features at 554 and 650 (broad) nm indicate formation of the $[Mn^{III}\text{–}(\mu\text{-}O)_2\text{–}Mn^{IV}]^{3+}$ complex of cyclen. Similarly, solutions containing pyclen gave rise to initial spectral features (Fig. S6†) consistent with a monomeric Mn^{III} species at short times (0–2 min): increasing absorbance in the UV, strong absorbance near λ ~400(sh) nm, weak broad feature with $\lambda = 525$ nm (see Fig. S7† for the absorbance spectrum of $[Mn(pyclen)Cl_2][ClO_4]$ for comparison). At times greater than 2 min after addition of the Mn salt, characteristic spectral features for $[Mn^{III}\text{–}(\mu\text{-}O)_2\text{–}Mn^{IV}]^{3+}$ (Fig. S6†) appear with a characteristic Mn^{III} d–d transition at 554 nm, broad absorbance centered at 650 nm (oxo-Mn^{IV} LMCT) and a weak, broad intervalence band at low energy (~750 nm).[56,57]

UV-visible absorbance spectroscopy studies in air saturated solutions of the cyclen and pyclen Mn complexes showed evidence for the formation of higher valent μ-O species. To further probe the species present during H_2O_2 disproportionation catalysis, the solution absorbance was monitored in 30 s increments following the addition of $\frac{1}{2}$ molar equivalents of H_2O_2 (relative to Mn^{II} added at the start). The solutions were allowed to age for 10 min in the case of pyclen or 30 min for cyclen prior to adding any H_2O_2. An initial $\frac{1}{2}$ molar equivalent of H_2O_2 was added at $t = 0$ of the experiment and additional $\frac{1}{2}$ molar equivalents every 10 min thereafter. In the case of pyclen (Fig. 6, top), absorbance features characteristic of $[Mn_2(pyclen)_2(\mu\text{-}O)_2]^{3+}$ grew more intense with increases in absorbance at 390, 554, and 650 nm. A maximum intensity for $[Mn_2(pyclen)_2(\mu\text{-}O)_2]^{3+}$ was observed after addition of the first half equivalent and bleached progressively over time. $[Mn_2(cyclen)_2(\mu\text{-}O)_2]^{3+}$ demonstrated similar behavior (Fig. 6, bottom), however, maximum intensity was observed following the addition of 1 full equivalent of H_2O_2 and decayed thereafter.

Fig. 7 tracks the absorbance measured at 554 nm indicative of the mixed valence $[Mn^{III}\text{–}(\mu\text{-}O)_2\text{–}Mn^{IV}]^{3+}$ species for both pyclen and cyclen during the addition of increasing molar equivalents of H_2O_2. In both cases, the addition of H_2O_2 resulted in a rapid initial increase in the absorbance at 554 nm, indicating formation of the $[Mn^{III}\text{–}(\mu\text{-}O)_2\text{–}Mn^{IV}]^{3+}$ complex. Additional $\frac{1}{2}$ molar equivalents of H_2O_2 added to the solution caused a gradual decrease in the absorbance at 554 nm with complete bleaching observed following the addition of 13 full equivalents to $[Mn_2(pyclen)_2(\mu\text{-}O)_2]^{3+}$ and 7 full equivalents to $[Mn_2(cyclen)_2(\mu\text{-}O)_2]^{3+}$. This trend implies better chemical stability of the pyclen complex under the catalytic conditions and matches the trend in TON measured in the presence of excess hydrogen peroxide with 22.5 ± 0.5 for $[Mn_2(pyclen)_2(\mu\text{-}O)_2]^{3+}$ and 9.5 ± 0.5 for $[Mn_2(cyclen)_2(\mu\text{-}O)_2]^{3+}$. Importantly, the persistence of the catalase activity of the complexes tracks with the presence of the $[Mn^{III}\text{–}(\mu\text{-}O)_2\text{–}Mn^{IV}]^{3+}$ species, indicating that this is an important intermediate in the catalytic mechanism.

Taken in conjunction with the activity for the related pyridinophane–Mn complexes reported by Smith and co-workers,[18,58]

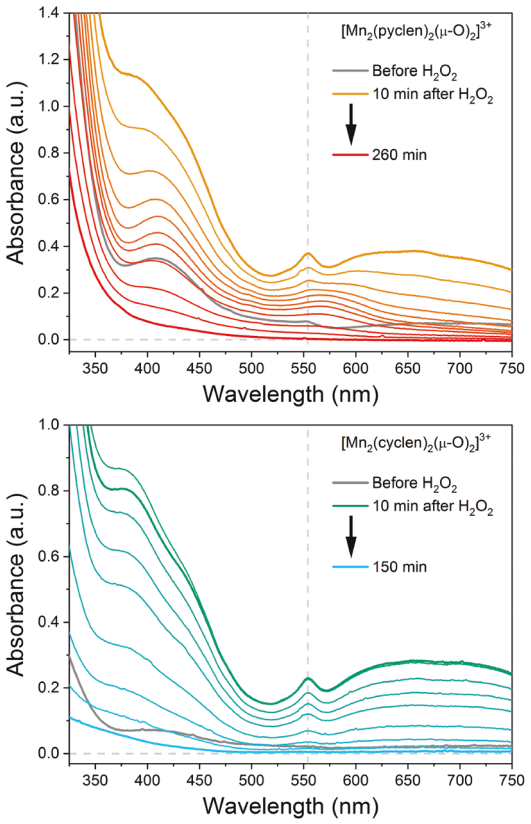

Fig. 6 Absorbance spectra in pH 8 buffered aqueous solution taken over an extended time as indicated for $[Mn_2(pyclen)_2(\mu\text{-}O)_2]^{3+}$ (top) and $[Mn_2(cyclen)_2(\mu\text{-}O)_2]^{3+}$ (bottom). In each plot, the spectrum of the solution following the aging period (10 min for pyclen, 30 min for cyclen) is shown in grey. At $t = 0$ min of the experiment, $\frac{1}{2}$ molar equivalent of H_2O_2 was added to solution and additional $\frac{1}{2}$ equivalents added every 10 min thereafter for the duration of the experiment. The orange spectrum for $[Mn_2(pyclen)_2(\mu\text{-}O)_2]^{3+}$ and green spectrum for $[Mn_2(cyclen)_2(\mu\text{-}O)_2]^{3+}$ were recorded immediately before the addition of the second $\frac{1}{2}$ equivalent of H_2O_2. The vertical grey dash indicates the wavelength monitored in Fig. 7.

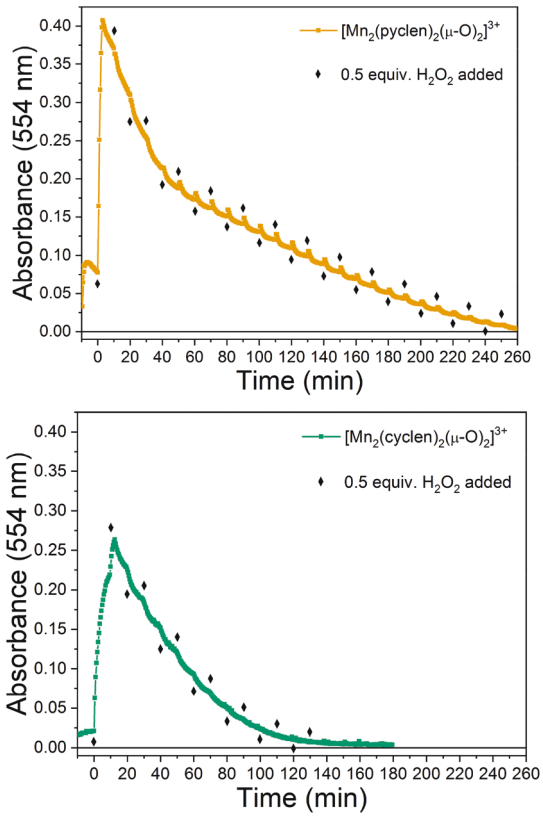

Fig. 7 Change of absorption intensity monitored at 554 nm (indicated with vertical dash line in Fig. 6) for $[Mn_2(pyclen)_2(\mu\text{-}O)_2]^{3+}$ (orange, top) and $[Mn_2(cyclen)_2(\mu\text{-}O)_2]^{3+}$ (green, bottom) recorded every 30 s during the experiment. The diamonds indicate the addition of a $\frac{1}{2}$ molar equivalents of H_2O_2 (to Mn^{II}) added every 10 min. Complete bleaching of the 554 nm feature was observed after the addition of 13 full equivalents of H_2O_2 for $[Mn_2(pyclen)_2(\mu\text{-}O)_2]^{3+}$ and 7 equivalents for $[Mn_2(cyclen)_2(\mu\text{-}O)_2]^{3+}$.

increasing the number of pyridine rings in the macrocycle progressively increases the stability of catalyst for H_2O_2 disproportionation with the TON increasing for cyclen < PyN_3 pyclen < Py_2N_2 pyridinophane. Interestingly, the activity of the Py_2N_2 pyridinophane complex has been reported as a monomeric catalyst,[18,58] whereas the spectroscopic investigation here with the cyclen and pyclen derivatives implicates the dimeric $[Mn^{III}\text{–}(\mu\text{-}O)_2\text{–}Mn^{IV}]^{3+}$ species during catalysis. The reliance of the catalytic activity on the presence of a dinuclear Mn complex resonates with the active site architecture of MnCAT. It is also notable that, while demonstrating the lowest TON of the series, the $[Mn_2(cyclen)_2(\mu\text{-}O)_2]^{3+}$ complex is competent for H_2O_2 disproportionation, which has not been previously reported for this well-studied complex.

Experimental

General methods

Caution! Perchlorate salts are explosive and should be handled with care; such compounds should never be heated as solids. All chemical reagents were purchased from either Millipore Sigma or Alfa Aesar and used without further purification unless otherwise indicated. Pyclen was isolated as the hydrochloride salt prior to metal ion complexation in accordance with previous reports.[23] Each reaction was carried out in H_2O. Elemental analyses were performed by Canadian Microanalytical Services Ltd.

Physical measurements

Electronic absorption spectra were collected between 190 nm and 1100 nm using a Cary 60 spectrophotometer (Agilent) and a 3 mL quartz cuvette with a path length of 1.0 cm. Molar extinction coefficients were calculated utilizing the Beer–Lambert law ($A = \varepsilon bc$). Infrared spectra were collected using an ATR Pro One attachment on a JASCO FT-IR 4600 spectrometer.

Electrochemistry

A BASi C3 cell stand with a glassy carbon working electrode, Ag/AgCl reference electrode, and platinum wire auxiliary electrode were used to conduct the electrochemical analysis of the Mn complexes. A standard three electrode cell under a blanket of N_2 at room temperature was used to obtain all voltammograms. $[Mn(pyclen)Cl_2][ClO_4]$ was evaluated in acetonitrile with 0.1 M of tetrabutylammonium perchlorate (TBAP) as the supporting electrolyte. $MnCl_2{\cdot}4H_2O$ was evaluated in 18 mQ H_2O with 0.1 M KCl as the supporting electrolyte and referenced to potassium ferricyanide ($K_3[Fe(CN)_6]$).

Potentiometric titrations

The concentration of cyclen as well as its protonation constants were determined by using pH-potentiometric titrations. A Metrohm 888 Titrando equipped with a Metrohm 6.0234.100 combined electrode was used to measure the pH in titration experiments. For the pH calibration of the electrode, KH-phthalate (pH 4.008) and borax (pH 9.177) buffers were used. The calculation of H^+ concentration from the measured pH values was performed with the use of the method proposed by Irving *et al.*[59] by titrating a 0.02 M HCl solution with a standardized NaOH solution (0.2 M). The differences between the measured and calculated pH values were used to obtain the $[H^+]$ from the pH-data collected in the titrations. The ion product of water was determined (pK_w = 13.714) from the same experiment in the pH range 11.40–12.00. The ionic strength in the titrated and thermostat controlled (25 °C) samples of 6.00 mL was kept constant and set to 0.15 M NaCl. The samples were stirred and N_2 was bubbled through the solution to avoid the effect of CO_2. The protonation constants of cyclen were determined by direct pH-potentiometric titration of 3 mM ligand solutions with a standardized NaOH solution in the pH range of 1.80–12.00. The $MnCl_2$ stock solution was prepared from the analytical grade tetrahydrate salt (Merck) and its concentration was determined by complexometric titration with standardized Na_2H_2EDTA and Eriochrome Black T indicator in the presence of ascorbic acid, triethanolamine, and ammonia/ammonium-chloride buffer (pH = 10). The stability constant of the Mn(II)-complexes were

determined using direct pH-potentiometric method by titrating samples with 1 : 1 metal-to-ligand ratios (the number of data pairs were between 120–140), allowing 1 min for the sample equilibration to occur. The titration was continued until the appearance of the precipitate (pH = 9–10). The protonation and stability constants were calculated from the titration data with the PSEQUAD program.[60]

Reaction of Mn complexes with H_2O_2 and quantification of O_2 evolution

The reactions were performed in a sealed pressure vessel (15 mL) equipped with a stir bar and a 3-way manifold valve. Two of the lines (PTFE tubing) were connected to the cell, one was used for N_2 and the other to inject the aliquot of H_2O_2. The pressure vessel was sealed using a PEEK bushing with custom machined ports. The ports enabled the use of threaded fittings (IDEX Health and Science) for sealing the gas tubing and microsensor in the reaction vessel. The pressure within the reactor was maintained at atmospheric level using a snorkel line with minimal loss of headspace gas during the catalytic studies. The O_2 microsensor was calibrated using N_2 and air (P_{O_2} = 0 mmHg and 159 mmHg) under atmospheric pressure.

The metal complexes were prepared in aqueous solutions at different pH values using stock solutions of the ligand of interest, buffer, and a metal solution of $MnCl_2{\cdot}4H_2O$. Trisodium citrate dihydrate (citrate), 4-(2-hydroxyethyl)piperazine-1-ethanesulfonic acid (HEPES) and Tris(hydroxymethyl) aminomethane (Tris) were used as buffers for pH 6, 7, and 8, respectively. The complexes were prepared by adding the corresponding amount of the stock solutions of ligand, buffer, and metal salt in a vial to achieve the targeted concentration for the H_2O_2 disproportionation studies ([ligand] = 2.04 mM; [Mn] = 2 mM; [buffer] = 50 mM).

The vessel was loaded with 1.5 mL of the solution detailed above and purged with N_2 gas prior to every measurement. The electrode signal was allowed to stabilize for 2 min to obtain a steady signal and then 0.5 mL of H_2O_2 solution was injected (600 mM, 50 mM buffer). The signal was recorded as ΔP_{O_2} *vs.* time until a plateau was achieved. Initial concentrations before starting the reaction were [ligand] = 1.53 mM (3.06 μmol), [Mn] = 1.5 mM (3 μmol) and [H_2O_2] = 150 mM (300 μmol).

Once the reaction was complete, the results were plotted to determine the turnover number (TON) and turnover frequency (TOF). The reaction was stopped when a visible plateau in the oxygen concentration was observed. To determine the timeframe used for TON and TOF calculation, the slope of the curve observed in Fig. 4 was calculated at different times. A decrease in the slope was related with a decrease of the activity. At pH 8, this decrease was observed after 10 min, but at lower pH values the reaction took longer to reach a plateau. The TON was calculated as the ratio between the moles of oxygen produced during the timeframe selected divided by moles of catalyst used. TOF was calculated as TON divided by the time. Fig. S4† shows the specific values of TOF at different timeframes.

Preparation of $[Mn(pyclen)Cl_2][ClO_4]$

Pyclen (100 mg, 0.317 mmol) was dissolved in 12 mL of H_2O. The pH of this solution was adjusted to 8 with a dilute solution of KOH. $Mn(ClO_4)_2$ (80 mg, 0.317 mmol) was then added to the pH adjusted solution. This mixture was stirred at room temperature for 12 h; the solution color gradually darkened from pale yellow to dark brown. After 12 h, this brown solution was filtered and solvent removed under reduced pressure to afford a dark brown/red tinged solid. The resulting solid was re-dissolved in CH_3CN (20 mL) and stirred, open to air, for 12 h. The resulting red-pink solution was filtered and the supernatant solvent was removed under reduced pressure to afford a pale pink-red powder (40.2 mg, 0.085 mmol, 57% yield). The bright pink-red powder was dissolved in CH_3CN and filtered, slow evaporation of the CH_3CN solution yielded X-ray quality crystals. Electronic absorption, λ_{max}/nm (ε/M^{-1} cm^{-1}); CH_3CN: 370 (sh, 153), 525 (46). Elemental Analysis; $[Mn(pyclen)Cl_2][ClO_4]{\cdot}2H_2O$ Found (calculated): C, 28.10 (28.25); H, 3.70 (4.74); N, 11.73 (11.98) %.

Preparation of $[Mn_2(pyclen)_2(\mu\text{-}O)_2][ClO_4]_3$

Pyclen (100 mg, 0.317 mmol) and $Mn(ClO_4)_2$ (80 mg, 0.317 mmol) were dissolved in 12 mL of H_2O. The pH of this solution was adjusted to 8 with a dilute solution of KOH. The resulting mixture was stirred at room temperature for 12 h; the solution color gradually darkened from pale yellow to dark brown to deep forest green. After 12 h, this green solution was filtered and solvent removed under reduced pressure to afford a dark green/brown solid. The resulting solid was redissolved in CH_3CN (20 mL) and stirred, open to air, for 12 h. The resulting solution, which was a dark green color, was filtered. The supernatant solvent was removed under reduced pressure to afford a dark green powder (90.0 mg, 0.097 mmol, 60% yield). The dark green powder was dissolved in H_2O and filtered, slow evaporation of the aqueous solution yielded X-ray quality crystals. Electronic absorption, λ_{max}/nm (ε/M^{-1} cm^{-1}); H_2O: 382 (652), 555(181), 665 (211), 800 (sh). $\nu(Mn_2O_2)$ (neat): 683 cm^{-1}. Elemental Analysis; $[Mn_2(pyclen)_2(\mu\text{-}O)_2][ClO_4]_3{\cdot}5H_2O$ Found (calculated): C, 28.37 (28.03); H, 4.53 (4.92); N, 11.86 (11.88) %.

X-band EPR spectroscopy and quantitative simulations

X-band (9 GHz) EPR spectra were recorded on a Bruker EMX Plus spectrometer equipped with a bimodal resonator (Bruker model 4116DM). Low-temperature measurements were made using an Oxford ESR900 cryostat and an Oxford ITC 503 temperature controller. A modulation frequency of 100 kHz was used for all EPR spectra. All experimental data used for spin-quantitation were collected under non-saturating conditions. Analysis of the EPR spectra utilized the general spin Hamiltonian (eqn (2)). Nuclear hyperfine interactions (A) are treated with second-order perturbation theory. Within the strong exchange limit ($J/D \gg 1$), the above spin Hamiltonian simplifies to eqn (3).

EPR spectra were simulated and quantified using Spin Count (ver. 6.2.6724.17768), written by Professor

M. P. Hendrich at Carnegie Mellon University. The simulations were generated with consideration of all intensity factors, both theoretical and experimental, to allow concentration determination of species. The only unknown factor relating the spin concentration to signal intensity was an instrumental factor that depended on the microwave detection system. However, this was determined by the spin standard, Cu(EDTA), prepared from a copper atomic absorption standard solution purchased from Sigma-Aldrich.

X-ray crystallography

A Leica MZ 75 microscope was used to identify samples suitable for analysis. A Bruker APEX-II CCD diffractometer was employed for crystal screening, unit cell determination, and data collection; which was obtained at 100 K. The Bruker D8 goniometer was controlled using the APEX2 software suite, v2014.11-0. The samples were optically centered with the aid of video camera so that no translations were observed as the crystal was rotated through all positions. The X-ray radiation employed was generated from a MoK_α sealed X-ray tube (λ = 0.71076) with a potential of 50 kV and a current of 30 mA; fitted with a graphite monochromator in the parallel mode (175 mm collimator with 0.5 mm pinholes). The crystal-to-detector distance was set to 50 mm, and the exposure time was 10 s per degree for all data sets at a scan width of 0.5°. The frames were integrated with the Bruker SAINT Software package using a narrow frame algorithm. Data were corrected for absorption effects using the multi-scan method SADABS. Using Olex2 the structure was solved with the ShelXS structure solution program using Direct Methods and refined with the SHELXL refinement package using Least Squares minimization. All hydrogen and non-hydrogen atoms were refined using anisotropic thermal parameters. The thermal ellipsoid molecular plots (50%) were produced using Olex2.

$[Mn(pyclen)Cl_2][ClO_4]$ structure determination

A translucent bright pink plate-like crystal (0.362 × 0.078 × 0.052 mm^3) was mounted on a 75 μm cryo-loop and used for X-ray crystallographic analysis. A total of 1104 frames were collected, and the data collection was 100% complete. The integration of the data used a monoclinic unit cell yielding a total of 28 307 reflections to a maximum θ angle of 30.12° (0.71 Å resolution) of which 4963 reflections were independent with the R_{int} = 8.29%. CCDC Deposition Number: 1963104.†

$[Mn_2(pyclen)_2(\mu\text{-}O)_2][ClO_4]_3$ structure determination

Slow evaporation of a dark green solution at room temperature afforded an opaque dark green block-like crystal (0.273 × 0.175 × 0.067 mm^3) that was mounted on a 100 μm cryo-loop and used for X-ray crystallographic analysis. A total of 1104 frames were collected, and the data collection was 100% complete. The integration of the data used a monoclinic unit cell yielding a total of 33 419 reflections to a maximum θ angle of 33.24° (0.65 Å resolution) of which 13 522 reflections were independent with the R_{int} = 4.35%. CCDC Deposition Number: 1963105.†

Conclusions

This report details the synthesis, structural analysis, and H_2O_2 disproportionation activity for a novel Mn complex with pyclen that is isolable as both the monomeric $[Mn(pyclen)Cl_2]^+$ and dimeric $[Mn_2(pyclen)_2(\mu\text{-}O)_2]^{3+}$ species. The reported *in situ* method for preparing this complex, as well as the related $[Mn_2(cyclen)_2(\mu\text{-}O)_2]^{3+}$, offers a facile method for assembling these complexes for catalytic studies. While modest in comparison with other Mn-based catalysts, quantification of the activity of both $[Mn_2(pyclen)_2(\mu\text{-}O)_2]^{3+}$ and $[Mn_2(cyclen)_2(\mu\text{-}O)_2]^{3+}$ mark these as important entrants to the series of macrocyclic MnCAT mimics reported to date and present a useful platform for interrogating the influence of the rigidity and electronic properties of the ligand on the catalytic functionality of the Mn complex.

Conflicts of interest

There are no conflicts to declare.

Acknowledgements

We are grateful for financial support from the National Institute of Health (NIGMS, R15GM123463 to K. N. G. and GM117511-02 to B. S. P.) and the National Science Foundation (CHE, 1709369 to B. S. P.). The authors are also grateful for financial support from TCU Andrews Institute of Mathematics & Science Education (to K. G.), Cambridge Isotope Laboratories, and TCU Research and Creativity Activity Grant (to K. G.). B. D. S. gratefully acknowledges start-up funding from Texas Christian University for support of this work.

References

1 M. Czerska, K. Mikolajewska, M. Zielinski, J. Gromadzinska and W. Wasowicz, Today's oxidative stress markers, *Med. Pr.*, 2015, **66**, 393.
2 E. Niedzielska, I. Smaga, M. Gawlik, A. Moniczewski, P. Stankowicz, J. Pera and M. Filip, Oxidative Stress in Neurodegenerative Diseases, *Mol. Neurobiol.*, 2016, **53**, 4094–4125.
3 A. I. Bush, The Metal Theory of Alzheimer's Disease, *J. Alzheimer's Dis.*, 2013, **33**, S277–S281.
4 M. Sastre, C. W. Ritchie and N. Hajji, Metal ions in Alzheimer's disease brain, *JSM Alzheimer's Dis. Relat. Dement.*, 2015, **2**, 1014.
5 D. K. V. Kumar, S. H. Choi, K. J. Washicosky, W. A. Eimer, S. Tucker, J. Ghofrani, A. Lefkowitz, G. McColl, L. E. Goldstein, R. E. Tanzi and R. D. Moir, Amyloid-β peptide protects against microbial infection in mouse and worm models of Alzheimer's disease, *Sci. Transl. Med.*, 2016, **8**, 340ra72.

6 F. Santilli, D. D'Ardes and G. Davi, Oxidative stress in chronic vascular disease: From prediction to prevention, *Vasc. Pharmacol.*, 2015, **74**, 23–37.
7 S. Gandhi and A. Y. Abramov, Mechanism of oxidative stress in neurodegeneration, *Oxid. Med. Cell. Longevity*, 2012, **2012**, 428010.
8 K. Dasuri, L. Zhang and J. N. Keller, Oxidative stress, neurodegeneration, and the balance of protein degradation and protein synthesis, *Free Radicals Biol. Med.*, 2013, **62**, 170–185.
9 A. Federico, E. Cardaioli, P. Da Pozzo, P. Formichi, G. N. Gallus and E. Radi, Mitochondria, oxidative stress and neurodegeneration, *J. Neurol. Sci.*, 2012, **322**, 254–262.
10 P. Naik, N. Fofaria, S. Prasad, R. K. Sajja, B. Weksler, P. O. Couraud, I. A. Romero and L. Cucullo, Oxidative and pro-inflammatory impact of regular and denicotinized cigarettes on blood brain barrier endothelial cells: is smoking reduced or nicotine-free products really safe?, *BMC Neurosci.*, 2014, **15**, 51.
11 A. Ivancich, V. V. Barynin and J.-L. Zimmermann, Pulsed EPR studies of the binuclear Mn(III)Mn(IV) center in catalase from Thermus thermophilus, *Biochemistry*, 1995, **34**, 6628–6639.
12 A. J. Wu, J. E. Penner-Hahn and V. L. Pecoraro, Structural, spectroscopic, and reactivity models for the manganese catalases, *Chem. Rev.*, 2004, **104**, 903–938.
13 S. Antonyuk, V. Melik-Adamyan, A. Popov, V. Lamzin, P. Hempstead, P. Harrison, P. Artymyuk and V. Barynin, Three-dimensional structure of the enzyme dimanganese catalase from Thermus thermophilus at 1 Å resolution, *Crystallogr. Rep.*, 2000, **45**, 105–116.
14 V. V. Barynin, M. M. Whittaker, S. V. Antonyuk, V. S. Lamzin, P. M. Harrison, P. J. Artymiuk and J. W. Whittaker, Crystal structure of manganese catalase from Lactobacillus plantarum, *Structure*, 2001, **9**, 725–738.
15 S. Signorella and C. Hureau, Bioinspired functional mimics of the manganese catalases, *Coord. Chem. Rev.*, 2012, **256**, 1229–1245.
16 J. D. Blakemore, R. H. Crabtree and G. W. Brudvig, Molecular Catalysts for Water Oxidation, *Chem. Rev.*, 2015, **115**, 12974–13005.
17 J. Yano and V. Yachandra, Mn4Ca cluster in photosynthesis: where and how water is oxidized to dioxygen, *Chem. Rev.*, 2014, **114**, 4175–4205.
18 W.-T. Lee, S. Xu, D. A. Dickie and J. M. Smith, A Robust Mn Catalyst for H_2O_2 Disproportionation in Aqueous Solution, *Eur. J. Inorg. Chem.*, 2013, **2013**, 3867–3873.
19 K. J. Brewer, A. Liegeois, J. W. Otvos, M. Calvin and L. O. Spreer, Synthesis and Properties of Two Bimetallic Mixed-Valence Di-u-oxo Manganese Complexes with Different Tetra-aza Macrocyclic Ligands, *J. Chem. Soc., Chem. Commun.*, 1988, 1219–1220.
20 R. Yan-Wei, L. Jun, Z. Feng-Xing, Z. Jin-Hua and G. Hui, Crystal Structure and Characterization of a New Mixed-valence Manganese (III/IV) Complex:[Mn2 (cyclen) 2 (μ-O) 2](ClO4) 3· 4H2O, *Chin. J. Chem.*, 2005, **23**, 418–420.
21 S. Xu, L. Bucinsky, M. Breza, J. Krzystek, C.-H. Chen, M. Pink, J. Telser and J. M. Smith, Ligand Substituent Effects in Manganese Pyridinophane Complexes: Implications for Oxygen-Evolving Catalysis, *Inorg. Chem.*, 2017, **56**, 14315–14325.
22 D. W. Crandell, S. Xu, J. M. Smith and M.-H. Baik, Intramolecular oxyl radical coupling promotes O–O bond formation in a homogeneous mononuclear Mn-based water oxidation catalyst: A computational mechanistic investigation, *Inorg. Chem.*, 2017, **56**, 4435–4445.
23 K. M. Lincoln, M. E. Offutt, T. D. Hayden, R. E. Saunders and K. N. Green, Structural, Spectral, and Electrochemical Properties of Nickel(II), Copper(II), and Zinc(II) Complexes Containing 12-Membered Pyridine- and Pyridol-Based Tetra-aza Macrocycles, *Inorg. Chem.*, 2014, **53**, 1406–1416.
24 K. M. Lincoln, T. E. Richardson, L. Rutter, P. Gonzalez, J. W. Simpkins and K. N. Green, An N-heterocyclic amine chelate capable of antioxidant capacity and amyloid disaggregation, *ACS Chem. Neurosci.*, 2012, **3**, 919–927.
25 S. M. Brewer, P. M. Palacios, H. M. Johnston, B. S. Pierce and K. N. Green, Isolation and Identification of the Pre-Catalyst in Iron-Catalyzed Direct Arylation of Pyrrole with Phenylboronic Acid, *Inorg. Chim. Acta*, 2018, **478**, 139–147.
26 H. M. Johnston, P. M. Palacios, B. S. Pierce and K. N. Green, Spectroscopic and solid-state evaluations of tetra-aza macrocyclic cobalt complexes with parallels to the classic cobalt(II) chloride equilibrium, *J. Coord. Chem.*, 2016, **69**, 1979–1989.
27 M. Regueiro-Figueroa, J. L. Barriada, A. Pallier, D. Esteban-Gómez, A. D. Blas, T. Rodríguez-Blas, É. Tóth and C. Platas-Iglesias, Stabilizing Divalent Europium in Aqueous Solution Using Size-Discrimination and Electrostatic Effects, *Inorg. Chem.*, 2015, **54**, 4940–4952.
28 A. E. Martell and R. M. Smith, *Critical stability constants*, Springer, 1974.
29 M. Botta, M. Ravera, A. Barge, M. Bottaro and D. Osella, Relationship between ligand structure and electrochemical and relaxometric properties of acyclic poly (aminocarboxylate) complexes of Eu(II), *Dalton Trans.*, 2003, 1628–1633.
30 C. Hureau, G. Blondin, M.-F. Charlot, C. Philouze, M. Nierlich, M. Cersario and E. Anxolaberhere-Mallart, Synthesis, Structure, and Characterization of New Mononuclear Mn(II) Complexes. Electrochemical Converstion into New Oxo-Bridged Mn_2(III,IV) Complexes. Role of Chloride Ions, *Inorg. Chem.*, 2005, **44**, 3669–3683.
31 A. Panja, N. Shaikh, P. Banerjee and B. Saha, Mechanistic disparity in the electron transfer reactions of thiosulfate with di-μ-oxo-bis (1, 4, 8, 11-tetraazacyclotetradecane)-dimanganese (III, IV) and di-μ-oxo-bis (1, 4, 7, 10-tetraazacyclododecane)-dimanganese (III, IV) complexes, *Int. J. Chem. Kinet.*, 2004, **36**, 119–128.
32 R. Dingle, The bisible and near-infrared spectrum of manganese(III) complexes, *Acta Chem. Scand.*, 1966, **20**, 33–44.
33 M. Suzuki, S. Tokura, M. Suhara and A. Uehara, Dinuclear Manganese(III,IV) and Manganese(IV,IV) Complexes with Tris(2-pyridylmethyl)amine, *Chem. Lett.*, 1988, 477–480.

34 F. A. Cotton, G. Wilkinson, C. A. Murillo and M. Bochmann, *Advanced Inorganic Chemistry*, John Wiley & Sons, Inc., New York, NY, 6th edn, 1999.
35 A. B. P. Lever, *Inorganic Electronic Spectroscopy*, Elsevier Publishing Company, Amsterdam, The Netherlands, 1968.
36 T. J. Hubin, J. M. McCormick, N. W. Alcock and D. H. Busch, Topologically Constrained Manganese(III) and Iron(III) Complexes of Two Cross-Bridged Tetraazamacrocycles, *Inorg. Chem.*, 2001, **40**, 435–444.
37 S. R. Cooper and M. Clavin, Mixed Valence Interactions in Di-u-oxo Bridged Manganese Complexes, *J. Am. Chem. Soc.*, 1977, **90**, 6623–6630.
38 M. Stebler, A. Ludi and H.-B. Burgi, $[(phen)_2Mn^{IV}(u\text{-}O)_2Mn^{III}(phen)_2](PF_6)_3$ CH_3CN and $[(phen)_2Mn^{IV}(u\text{-}O)_2Mn^{IV}(phen)_2](ClO_4)_4$ CH_3CN (phen = 1,10-Phenanthroline): Crystal Structure Analyses at 100 K, Interpretation of Disorder, and Optical, Magnetic, and Electrochemical Results, *Inorg. Chem.*, 1986, **25**, 4743–4750.
39 K. S. Hagen, W. H. Armstrong and H. Hope, Isolation of a Bis-Oxo-Bridged $Mn^{III}Mn^{IV}$ Intermediate by Regulated Air Oxidation. Synthesis, Structure, and Properties of $[Mn_2O_2(tren)_2](CF_3SO_3)_3$, *Inorg. Chem.*, 1988, **27**, 967–969.
40 K. J. Brewer, M. Clavin, R. S. Lumpkin, J. W. Otvos and L. O. Spreer, Synthesis, Structure, and Characterization of a Mixed-Valence Manganese(III)-Manganese(IV) Bis(u-oxo) Complex with a Macrocyclic Tetraaza Ligand, *Inorg. Chem.*, 1989, **28**, 4446–4451.
41 P. A. Goodson, J. Glerup, K. Michelsen and E. Pedersen, Binuclear Bis(u-oxo)dimanganese(III,IV) and -(IV,IV) Complexes with N,N'-Bis(2-pyridylmethyl)-1,2-ethanediamine, *Inorg. Chem.*, 1990, **29**, 503–508.
42 P. A. Goodson and D. J. Hodgson, Synthesis and Characterization of the Mixed-valent Complex Ion Di-u-oxobis(1,4,8,11-tetraazacyclotetradecane)dimanganese(III, IV), $[(cyclam)MnO]_2^{3+}$, *Inorg. Chim. Acta*, 1990, 49–57.
43 M. B. Robin and P. Day, Mixed valence chemistry: A survey and classification, *Adv. Inorg. Chem. Radiochem.*, 1967, **10**, 247–422.
44 D. Tomczyk, G. Andrijewski, L. Nowak, P. Urbaniak and D. Sroczyński, Spectroscopic and electrochemical properties of mononuclear Mn(III) complex and of binuclear di-μ-oxo bridged Mn(III) and Mn(IV) complex with isocyclam, *Inorg. Chim. Acta*, 2012, **390**, 70–78.
45 P. A. Goodson, D. J. Hodgson, J. Glerup, K. Michelsen and H. Weihe, Syntheses and characterization of binuclear manganese (III, IV) and (IV, IV) complexes with 1, 4, 7, 10-tetraazacyclododecane (cyclen), *Inorg. Chim. Acta*, 1992, **197**, 141–147.
46 P. A. Goodson and D. J. Hodgson, Synthesis and characterization of a bis (oxo)-bridged MN (III) Mn(III) complex, bis (. mu.-oxo) bis [N, N'-bis ((6-methylpyrid-2-yl) methyl) ethane-1, 2-diamine] dimanganese(III) perchlorate, *Inorg. Chem.*, 1989, **28**, 3606–3608.
47 A. Haddy, G. S. Waldo, R. H. Sands and J. E. Penner-Hahn, Simulation of Multifrequency EPR Spectra from Mn(III)/Mn (IV) Catalase of Lactobacillus plantarum Using a New Approach Based on Perturbation Theory, *Inorg. Chem.*, 1994, **33**, 2677–2682.
48 M. Zheng, S. V. Khangulov, G. C. Dismukes and V. V. Barynin, Electronic structure of dimanganese(II,III) and dimanganese(III,IV) complexes and dimanganese catalase enzyme: a general EPR spectral simulation approach, *Inorg. Chem.*, 1994, **33**, 382–387.
49 C. Hureau, G. Blondin, M. Cesario and S. Un, Direct Measurement of the Hyperfine and g-Tensors of a Mn(III)–Mn(IV) Complex in Polycrystalline and Frozen Solution Samples by High-Field EPR, *J. Am. Chem. Soc.*, 2003, **125**, 11637–11645.
50 J. Yano, K. Sauer, J.-J. Girerd and V. K. Yachandra, Single Crystal X- and Q-Band EPR Spectroscopy of a Binuclear Mn_2(III,IV) Complex Relevant to the Oxygen-Evolving Complex of Photosystem II, *J. Am. Chem. Soc.*, 2004, **126**, 7486–7495.
51 C. Hureau, G. Blondin, M. Cesario and S. Un, Direct Measurement of the Hyperfine and g-Tensors of a Mn(III)–Mn(IV) Complex in Polycrystalline and Frozen Solution Samples by High-Field EPR, *J. Am. Chem. Soc.*, 2003, **125**, 11637–11645.
52 S. Xu, L. Bucinsky, M. Breza, J. Krzystek, C. H. Chen, M. Pink, J. Telser and J. M. Smith, Ligand Substituent Effects in Manganese Pyridinophane Complexes: Implications for Oxygen-Evolving Catalysis, *Inorg. Chem.*, 2017, **56**, 14315–14325.
53 K. Pota, Z. Garda, F. K. Kálmán, J. L. Barriada, D. Esteban-Gómez, C. Platas-Iglesias, I. Tóth, E. Brücher and G. Tircsó, Taking the next step toward inert Mn^{2+} complexes of open-chain ligands: the case of the rigid PhDTA ligand, *New J. Chem.*, 2018, **42**, 8001–8011.
54 F. K. Kálmán, A. Végh, M. Regueiro-Figueroa, É. Tóth, C. Platas-Iglesias and G. Tircsó, H4octapa: Highly Stable Complexation of Lanthanide(III) Ions and Copper(II), *Inorg. Chem.*, 2015, **54**, 2345–2356.
55 K. N. Green, K. Pota, G. Tircsó, R. A. Gogolák, O. Kinsinger, C. Davda, K. Blain, S. M. Brewer, P. Gonzalez, H. M. Johnston and G. Akkaraju, Dialing in on pharmacological features for a therapeutic antioxidant small molecule, *Dalton Trans.*, 2019, **48**, 12430–12439.
56 P. A. Goodson, A. R. Oki, J. Glerup and D. J. Hodgson, Design, synthesis, and characterization of bis (. mu.-oxo) dimanganese (III, III) complexes. Steric and electronic control of redox potentials, *J. Am. Chem. Soc.*, 1990, **112**, 6248–6254.
57 S. R. Cooper and M. Calvin, Mixed valence interactions in di-. mu.-oxo bridged manganese complexes, *J. Am. Chem. Soc.*, 1977, **99**, 6623–6630.
58 W. T. Lee, S. B. Munoz 3rd, D. A. Dickie and J. M. Smith, Ligand modification transforms a catalase mimic into a water oxidation catalyst, *Angew. Chem., Int. Ed.*, 2014, **53**, 9856–9859.
59 H. Irving, M. Miles and L. Pettit, A study of some problems in determining the stoichiometric proton dissociation constants of complexes by potentiometric titrations using a glass electrode, *Anal. Chim. Acta*, 1967, **38**, 475–488.
60 L. Zékány and I. Nagypál, in *Computational Methods for the Determination of Formation Constants*, Springer, 1985, pp. 291–353.

